

Investigation of a large change in deformation for the γ -soft nucleus ^{136}Sm

F. S. Babra,¹ R. Palit¹, S. Rajbanshi², S. Jehangir,³ B. Das¹, G. H. Bhat,^{4,5} J. A. Sheikh,⁵ S. Biswas,¹ U. Garg,⁶ Md. S. R. Laskar¹, C. Palshetkar,¹ S. Saha,¹ J. Sethi,¹ and P. Singh¹

¹*Department of Nuclear and Atomic Physics, Tata Institute of Fundamental Research, Mumbai 400005, India*

²*Presidency University, Kolkata 700073, India*

³*Department of Physics, National Institute of Technology, Srinagar 190006, India*

⁴*Department of Physics, SP College Srinagar, Jammu and Kashmir 190001, India*

⁵*Cluster University Srinagar, Jammu and Kashmir, Srinagar, Goji Bagh 190008, India*

⁶*Physics Department, University of Notre Dame, Notre Dame, Indiana 46556, USA*



(Received 8 August 2019; published 7 November 2019)

Lifetimes of excited states of the ground-state rotational band in the ^{136}Sm nucleus have been measured up to $I^\pi = 20^+$ using the Doppler-shift attenuation method. The states were populated in the reaction $^{107}\text{Ag}(^{32}\text{S}, 1p2n)$ at 145-MeV beam energy and the γ rays emitted from the excited states were detected using the Indian National Gamma Array at the Tata Institute of Fundamental Research, Mumbai. The extracted transitional quadrupole moments indicate a reduction of collectivity with increasing spin after the band crossing. The results have been compared with the predictions of the cranked shell model as well as the triaxial projected shell-model calculations and indicate that the nucleus evolves from prolate γ -soft to a stable triaxially deformed shape after the first and the second crossing involving $\pi h_{11/2}^2$ and $\pi h_{11/2}^2 \otimes \nu h_{11/2}^2$ configurations, respectively.

DOI: [10.1103/PhysRevC.100.054308](https://doi.org/10.1103/PhysRevC.100.054308)

I. INTRODUCTION

The evolution of nuclear deformation for neutron-deficient nuclei in the mass $A \approx 130$ region has attracted considerable interest in recent years. The ground states of nuclei in the vicinity of region $Z = 62$ and $N = 74$ are predicted to have axial asymmetry [1]. At higher excited states, shape coexistence and evolution may occur due to competing driving forces from valence protons and neutrons [2]. Heavier Sm isotopes below the $N = 82$ shell closure have been shown to exhibit deformed triaxial shapes with significant γ softness, while the lighter isotopes are prolate deformed at lower-excitation energies [3–9]. The observation of characteristic low-lying γ bands is a manifestation of triaxial deformation in $^{136-140}\text{Sm}$ [1,10,11]. In ^{138}Sm , significant triaxiality has been observed [12]. The total Routhian surface (TRS) calculations suggest that ^{136}Sm is a truly transitional γ -soft nucleus between the prolate ^{134}Sm and the triaxial ^{138}Sm isotopes. The transitional nuclei are susceptible to shape changes driven by rotational alignment of quasiparticle pairs involving high- j orbitals which can polarize the γ -soft cores to specific values of γ .

Lifetime measurements of the excited states are a very useful tool to probe the evolution of nuclear shapes. However, the experimental data on lifetime measurements for even-even Sm isotopes is limited up to low and medium spin. Previous work on the yrast band of ^{136}Sm up to $I^\pi = 24^+$ has been published in Refs. [6,13]; however, lifetimes of only lower members of the ground-state rotational band have been measured [14–17]. The motivation of the present work is to probe the shape evolution in the yrast band of ^{136}Sm beyond

the band crossing to see the effect of proton and neutron alignments via lifetimes of the excited states. Investigation of such shape changes with increasing spin is of contemporary interest, because it can generate various geometries of the core and particle angular momenta, which are essential for novel excitation modes.

The present work reports lifetime measurement of excited yrast states in ^{136}Sm using the Doppler-shift attenuation method (DSAM). The deduced Q_t values provide an understanding of the evolution of collectivity along the yrast band. The experimental results are compared with those of TRS calculations and triaxial projected shell model (TPSM) calculations to probe the shape evolution or the shape coexistence associated with medium to high spins along the band.

II. EXPERIMENTAL DETAILS AND RESULTS

The quadrupole structure of interest in ^{136}Sm has been investigated through the fusion evaporation reaction $^{107}\text{Ag}(^{32}\text{S}, 1p2n)$ using the Indian National Gamma Array (INGA) facility at the Tata Institute of Fundamental Research (TIFR), Mumbai. The ^{32}S 145-MeV beam of energy was bombarded on ^{107}Ag , prepared by rolling a 1.2 mg/cm² ^{107}Ag foil onto a 12.5 mg/cm² thick ^{197}Au backing to stop all recoiling nuclei produced in the reaction. The γ rays emitted from the residual nuclei were detected with 18 Compton-suppressed high-purity germanium Clover detectors that were arranged at angles (number of detectors) 23° (2), 40° (2), 65° (2), 90° (4), 115° (2), 140° (3), and 157° (3) with respect to the beam direction. Two- and higher-fold coincidence events were recorded using a fast digital data acquisition system based on

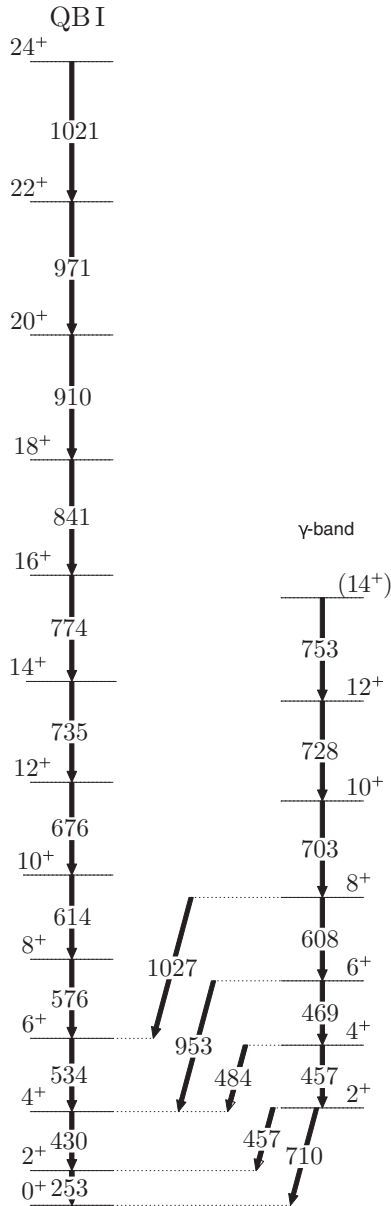


FIG. 1. Partial level scheme of ^{136}Sm showing the yrast band and γ -vibration rotational band.

the Pixie-16 module of XIA-LLC [18,19]. The time-stamped data were sorted using the MultipARAMeter time-stamped-based COincidence Search (MARCOS) [19] program developed at TIFR, Mumbai. The γ -ray energy calibration and relative photopeak efficiencies were obtained using standard ^{152}Eu and ^{133}Ba radioactive sources. The coincidence events were arranged into E_γ - E_γ symmetric and different angle-dependent matrices. RADWARE [20] has been used to obtain the coincidence spectra used in the subsequent analysis.

A partial level scheme of ^{136}Sm obtained from the present investigation is shown in Fig. 1. The level scheme consists of the yrast [quadrupole band (QB) I] and γ bands and is in agreement with previous work [6,13]. The yrast and γ bands have been shown up to spins $I^\pi = 24^+$ and 14^+ , respectively. All the previously reported γ -ray transitions of the yrast

TABLE I. Experimentally deduced lifetimes and transitional quadrupole moment (Q_t) values for the ground-state band excited states in ^{136}Sm .

E_γ (keV)	I (\hbar)	τ (ps)	Q_t (e b)
576	8^+	$1.23^{+0.08}_{-0.08}$	$5.66^{+0.19}_{-0.19}$
614	10^+	$0.89^{+0.25}_{-0.25}$	$5.59^{+0.78}_{-0.79}$
676	12^+	$0.52^{+0.04}_{-0.04}$	$5.70^{+0.21}_{-0.20}$
735	14^+	$0.38^{+0.05}_{-0.05}$	$5.38^{+0.34}_{-0.33}$
774	16^+	$0.36^{+0.05}_{-0.05}$	$4.85^{+0.34}_{-0.32}$
841	18^+	$0.22^{+0.03}_{-0.03}$	$5.05^{+0.37}_{-0.33}$
910	20^+	$<0.16(4)$	$>4.74(55)$

sequence and the γ band have been observed in the present work.

Doppler-broadened shapes of seven quadrupole transitions of the yrast band, decaying from $I^\pi = 20^+$ to $I^\pi = 8^+$ states have been observed (see Figs. 2, 3, and 4). To perform the line-shape analysis, angle-dependent E_γ - E_γ asymmetric matrices were used to construct the background-subtracted coincidence spectra from all the detector angles. The coincidence spectra obtained from both upper and lower gates along the band were used to fit the lineshapes of the transitions. Lifetimes of these levels were extracted by analyzing the observed shapes of the transitions, depopulating the state of interest, with the help of the LINESHAPE code developed by Wells and Johnson [21]. Tables of shell-corrected Northcliffe and Schilling [22] electronic stopping power and range were used for the energy-loss calculations of the residual nuclei moving through the target-backing combination. In the fitting process of the observed lineshape in the experimental spectra obtained from the gate on the transition below, the side-feeding to each level was modeled as a cascade of seven transitions having a fixed moment of inertia which was close to the yrast band [21]. The topmost transition of the band, whose shape was observed clearly in experimental spectra, had been assigned 100% side-feeding intensity. Thus, only an effective lifetime was obtained for the topmost 20^+ states. The side-feeding intensity for each state in the cascade was obtained from the relative intensity of the transitions populating and depopulating through the level and was found to be around 25% for higher spins. For states with $I^\pi = 8^+$, no side-feeding was considered owing to the fact that the 576-keV spectra were constructed with a gate on transitions above the level of interest. Lineshapes of all other transitions were obtained with gates on lower transitions in the cascade.

Lineshapes of 576-, 614-, and 676- keV transitions were obtained by fitting the 23° , 90° , and 157° spectra simultaneously as shown in Fig. 2. For the 735-, 774-, and 841-keV transitions, lineshapes were fitted for all the detector angles (see Fig. 3), while for the 910-keV transitions, 40° , 65° , 90° , 115° , and 140° spectra were used (see Fig. 4). Uncertainties in the extracted lifetimes were determined from the behavior of χ^2 in the vicinity of the minimum. Detailed descriptions of the lineshape-fitting process can be found in Refs. [23,24]. The extracted level lifetimes are presented in Table I. The

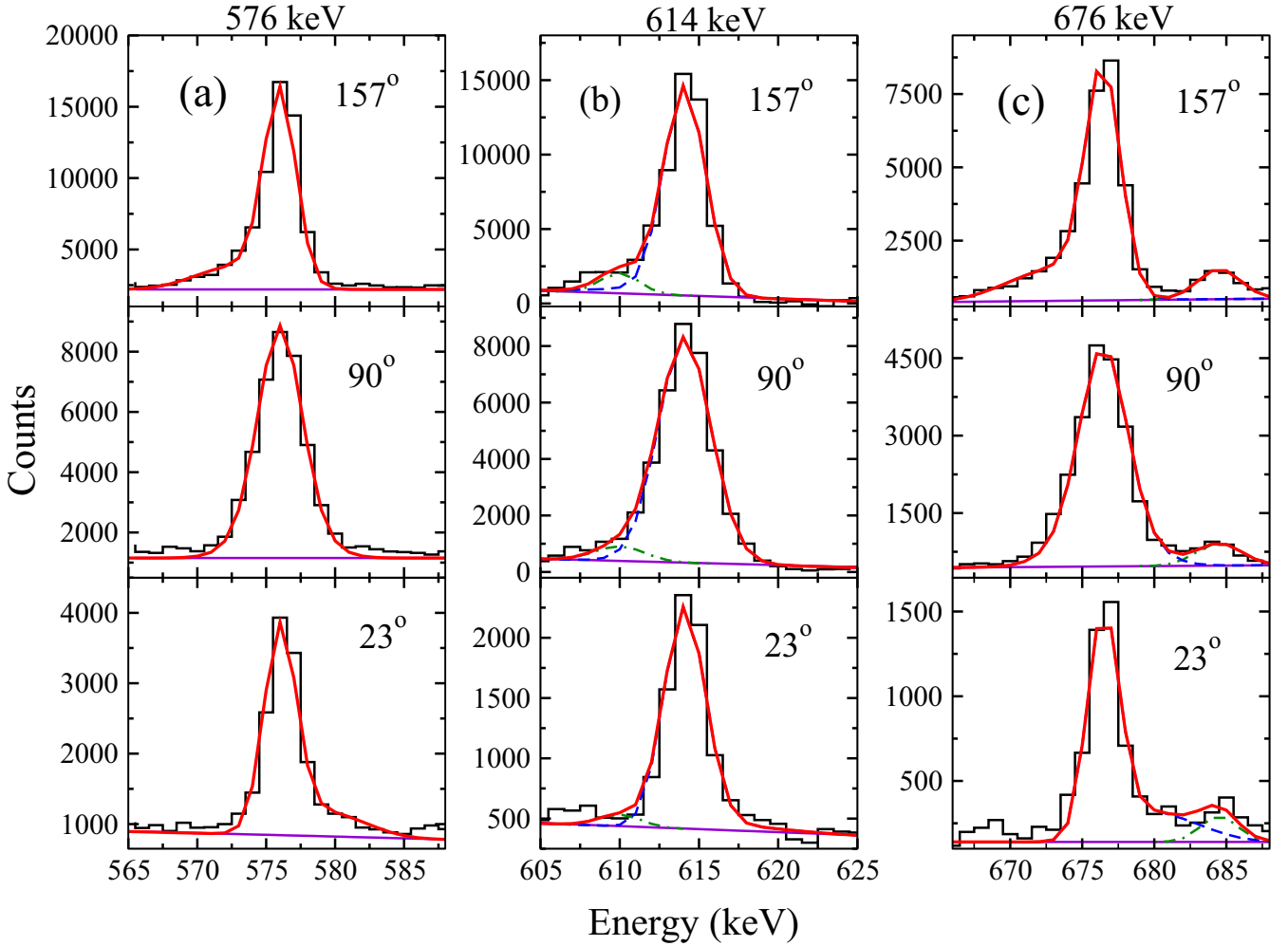


FIG. 2. Fitted lineshape spectra for (a) 576-keV, (b) 614-keV, and (c) 676-keV quadrupole transitions in the yrast band of ^{136}Sm . The top, middle, and bottom rows correspond to the shapes in 157° , 90° , and 23° detectors, respectively. The lineshapes of the above mentioned γ transitions, contaminant peaks, and total lineshapes are depicted as dashed, dot-dashed, and solid lines, respectively.

contribution from the systematic errors due to the stopping power calculations was not included and can be as large as 15%.

The experimental transition quadrupole moment values, Q_t , in electron barns were obtained from the measured lifetimes using the following relation:

$$Q_t = \sqrt{\frac{16\pi}{5} \frac{1}{(12.33)\tau E_\gamma^5 \langle J_i K 20 | J_f K \rangle^2}}, \quad (1)$$

where E_γ is the transition energy in MeV, τ is the mean lifetime in picoseconds measured for the E_γ decaying level, K is the projection of total angular momentum on the symmetry axis, and $\langle J_i K 20 | J_f K \rangle$ is a Clebsch-Gordon coefficient for the transition decaying from I (I_i) to $I - 2$ (I_f). Here, $K = 0$ which is a good approximation in even-even nuclei.

III. DISCUSSION

Intrinsic structure of the ground-state band of ^{136}Sm has been interpreted within the framework of the cranked

shell model and TPSM calculations. The quasiparticle alignment (i_x) and the dynamic moment of inertia ($J^{(2)}$) as a function of the rotational frequency (ω) are shown in Fig. 5. The value of i_x is obtained by subtracting the reference [$I_{x,\text{ref}}(\omega) = (J_0 + \omega^2 J_1)\omega$] from its absolute value [$i_x = \sqrt{I(I+1) - K^2}$]:

$$i_x(\omega) = I_x(\omega) - I_{x,\text{ref}}(\omega), \quad (2)$$

where $I_x(\omega)$ is the x component (rotational component) of the total angular momentum. The Harris parameters $J_0 = 12.5\hbar^2 \text{ MeV}^{-1}$ and $J_1 = 20\hbar^4 \text{ MeV}^{-3}$ have been used. It is evident from Fig. 5 that band QB I undergoes three band crossings at frequencies $\omega \approx 0.30, 0.38$, and 0.50 MeV , respectively. These may be due to the crossing of the quasiparticles in the $h_{11/2}$ orbitals of the proton and/or neutron sector in ^{136}Sm . While the alignments of ^{138}Sm indicate two back-bendings, the $^{132,134,136}\text{Sm}$ isotopes show a gradual increase in alignment instead [6]. This indicates a change in the nature of the interband interactions around $N = 74$ for the even-even Sm isotopes.

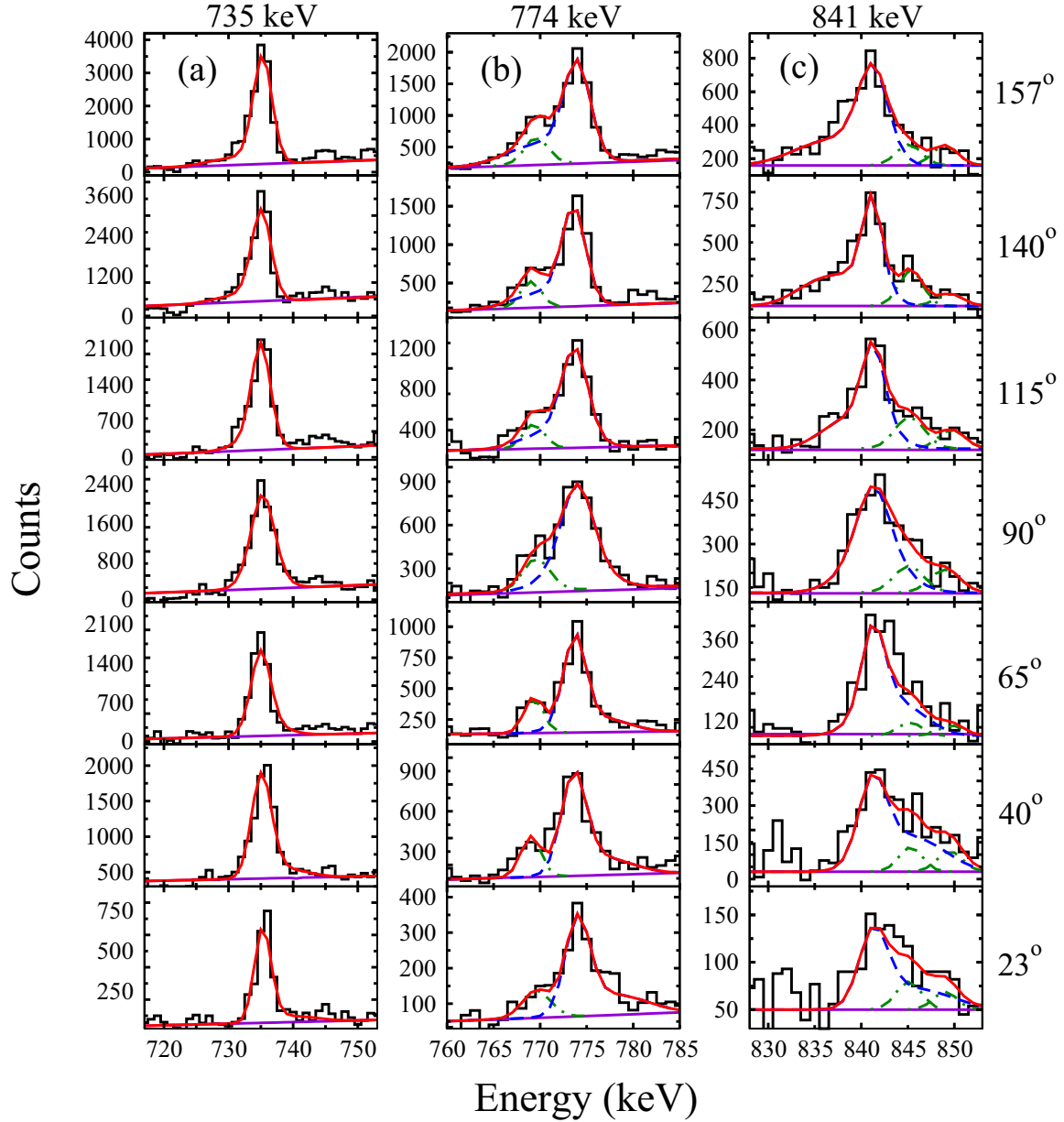


FIG. 3. Fitted lineshape spectra for 735-keV, 774-keV, and 841-keV quadrupole transitions in the yrast band of ^{136}Sm . Detector angles corresponding to the lineshapes are mentioned to the right. The lineshapes of the above mentioned γ transitions, contaminant peaks, and total lineshapes are depicted as dashed, dot-dashed, and solid lines, respectively.

To understand the observed crossings, we have calculated the neutron and proton quasiparticle energies as a function of the rotational frequency (ω) at typical values of the deformation parameters $\beta_2 = 0.25$, $\beta_4 = 0.02$, and $\gamma = -15^\circ$ and presented them in Fig. 6. The calculations show that the proton quasiparticle crossing for the $h_{11/2}$ orbital occurs at rotational energies ($\hbar\omega$) of ≈ 0.30 MeV (first crossing) with the configuration $\pi 1/2^- [550] \otimes 3/2^- [541]$ and ≈ 0.50 MeV (second crossing), while the neutron quasiparticle crosses at $\hbar\omega \approx 0.40$ MeV (first crossing) with the configuration $\pi 3/2^- [541] 3/2^- [541] \otimes \nu 7/2^- [523] 9/2^- [514]$ and ≈ 0.55 MeV (second crossing) (Fig. 6). Above $\hbar\omega \approx 0.60$ MeV in the neutron sector, there exist several crossings

due to both positive and negative parities of the orbitals and these are beyond the scope of the present discussion. Thus, the observed experimental crossings at $\hbar\omega \approx 0.30$ and 0.38 MeV (Fig. 5) are most likely due to the crossing of the $h_{11/2}$ proton and $h_{11/2}$ neutron orbitals, respectively, for the band QB I. The origin of the experimentally observed third crossing at $\omega \approx 0.50$ MeV may lie in the proton sector because the proton quasiparticle orbitals show a crossing around this frequency (Fig. 6). The band crossings observed in the ground-state band, involving the $\pi h_{11/2}^2 \otimes h_{11/2}^0$, $\pi h_{11/2}^2 \otimes \nu h_{11/2}^2$, and $\pi h_{11/2}^4 \otimes \nu h_{11/2}^2$ configurations would be expected to induce shape variation with increasing spin.

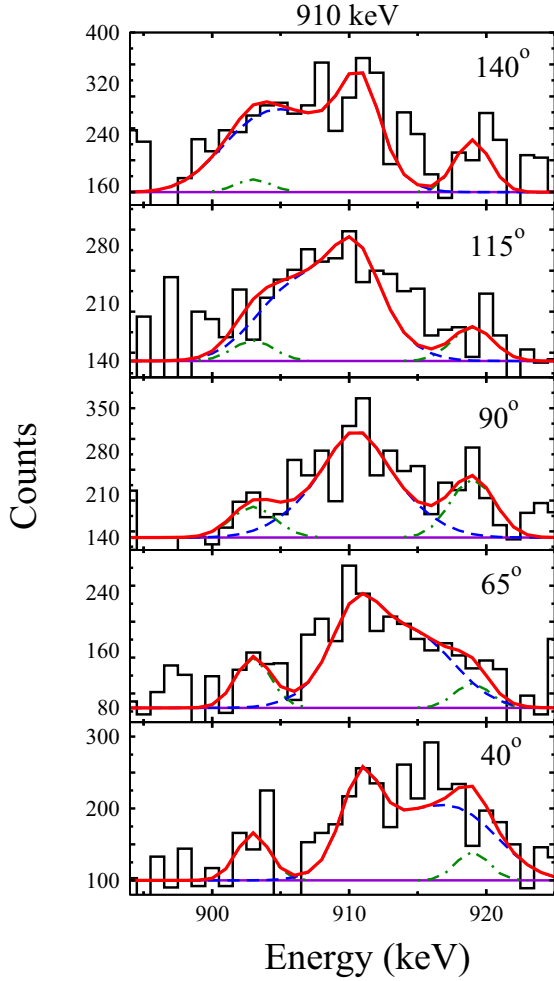


FIG. 4. Fitted lineshape spectra for 910-keV transitions in the yrast band of ^{136}Sm . Detector angles corresponding to the lineshapes are mentioned within the panels. The lineshapes of the above mentioned γ transitions, contaminant peaks, and total lineshapes are depicted as dashed, dot-dashed, and solid lines, respectively.

A. Total Routhian surface calculations

TRS calculations [25,26] with a positive ($\alpha = 0$) signature have been carried out to understand the shape of the ^{136}Sm nucleus associated with the configurations assigned to the band QB I. The contour plots of the TRS calculations of the abovementioned configurations of the positive-parity structure are presented in Fig. 7. The TRS has been calculated at each frequency, ω , in the β_2 - γ plane, with minimization on β_4 , considering the macroscopic liquid-drop energy of the nucleus, the shell correction, and the pairing energy. The single-particle energies were obtained from the Woods-Saxon potential and the pairing included a monopole and a double-stretched quadrupole interaction [25,26].

The nucleus has a γ -soft shape around the minimum with $\beta_2 \approx 0.30$ and $\gamma \approx 0^\circ$ at low frequencies with $\omega = 0.10$ – 0.30 MeV associated with the band QB I as seen in Fig. 7(a). This minimum becomes unfavorable above $\omega \approx 0.30$ and subsequently disappears at higher ω values. Another stable triaxial minimum ($\beta_2 \approx 0.22$, $\gamma \approx -25^\circ$) appears at

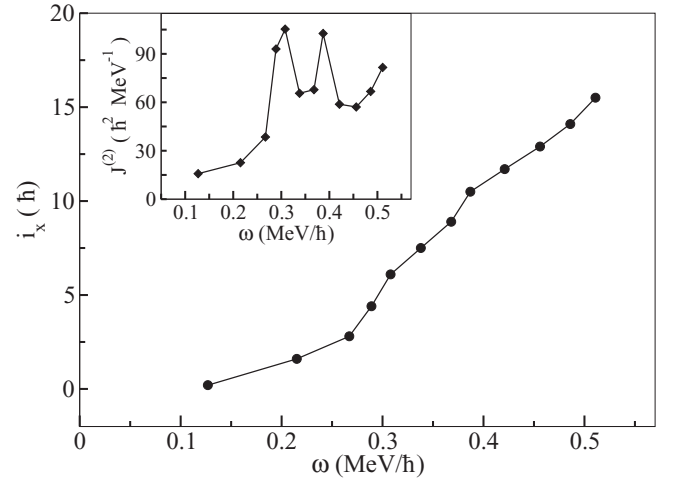


FIG. 5. Variation of the experimental aligned angular momentum (i_x) against the rotational frequency (ω) for the quadrupole band QB I in ^{136}Sm . Harris parameters used in the calculation of i_x are $J_0 = 12.5\hbar^2 \text{ MeV}^{-1}$ and $J_1 = 20\hbar^4 \text{ MeV}^{-3}$. The inset shows the character of the dynamic moment of inertia ($J^{(2)}$) with ω for the band QB I.

$\omega \approx 0.30$ and continues up to $\omega \approx 0.60$ value [see Figs. 7(b), 7(c), and 7(d)]. At higher rotational frequencies, a highly deformed prolate shape ($\beta_2 \approx 0.38$, $\gamma \approx 0^\circ$) becomes energetically favored as seen in Fig. 7(d). Such a minimum will be associated with a strongly deformed structure that has indeed been observed in a recent investigation of ^{136}Sm [13]. There also exists a collective oblate minimum ($\beta_2 \approx 0.22$, $\gamma \approx -60^\circ$) that appears at and above $\hbar\omega \approx 0.50$ MeV.

The intrinsic shape of the nucleus associated with the quadrupole band QB I has been explored by calculating the quadrupole moment Q_t from the minimized β_2 and γ values as

$$Q_t = \frac{3}{\sqrt{5}\pi} ZR^2 \beta_2 (1 + 0.16\beta_2) \frac{\cos(\gamma + 30^\circ)}{\cos 30^\circ} \quad (3)$$

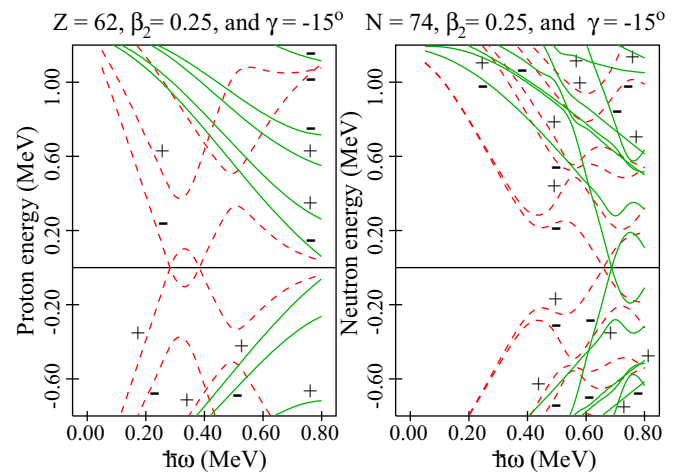


FIG. 6. Proton and neutron quasiparticle energies for ^{136}Sm . The positive and negative parity orbitals are represented by the solid and dashed black lines, respectively. The positive and negative signatures are indicated by the “+” and “−” signs, respectively.

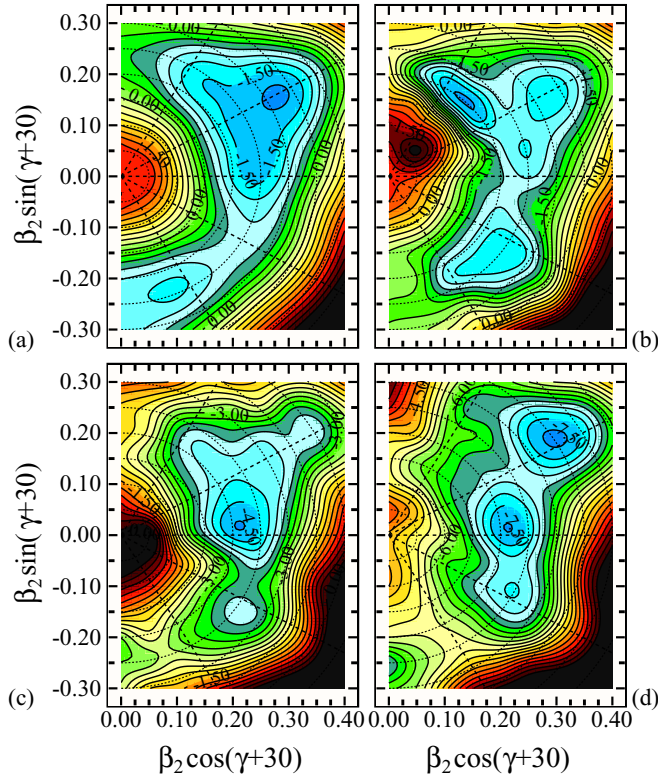


FIG. 7. Contour plots having the 0.250-MeV energy different between two consecutive contours of the TRS calculations for the positive-parity quadrupole band QB I in ^{136}Sm . The rotational frequencies ($\hbar\omega$) for the calculations are (a) 0.210, (b) 0.290, (c) 0.390, and (d) 0.510 MeV.

and compared with the experimentally measured values at different rotational frequencies, as depicted in Fig. 8. Here, β_2 and γ are the deformation parameters, whereas Z and R are the proton number and the radius of the nucleus of interest, ^{136}Sm , respectively.

The Q_t values for seven states above $I^\pi = 6^+$ have been extracted from the present lifetime measurements using the DSAM. These Q_t values are plotted in Fig. 8(a) along with the values reported in Ref. [14]. Within the experimental error, the present Q_t values for $I^\pi = 8^+$ and 10^+ states agree with the values reported earlier in Ref. [14]. The calculated Q_t values corresponding to the three minima observed in the energy surface calculations at various frequencies are also shown in Fig. 8(a).

Within the experimental uncertainties, the Q_t values at low frequency (before first crossing) remain nearly constant, though the present Q_t values for the 8^+ , 10^+ , and 12^+ states are slightly higher than that of the 2^+ and 4^+ states reported in Ref. [14]. This trend has been fairly well reproduced with the calculated values arising from the prolate ($\beta_2 \approx 0.30$ and $\gamma \approx 0^\circ$) minimum in the TRS framework. The measured Q_t values gradually decrease after $I^\pi = 12^+$, indicating a loss of collectivity. This observed variation of the experimental Q_t values for the states after the first crossing is well explained within the theoretically calculated results for the triaxial minimum with $\beta_2 \approx 0.22$ and $\gamma \approx -25^\circ$. However,

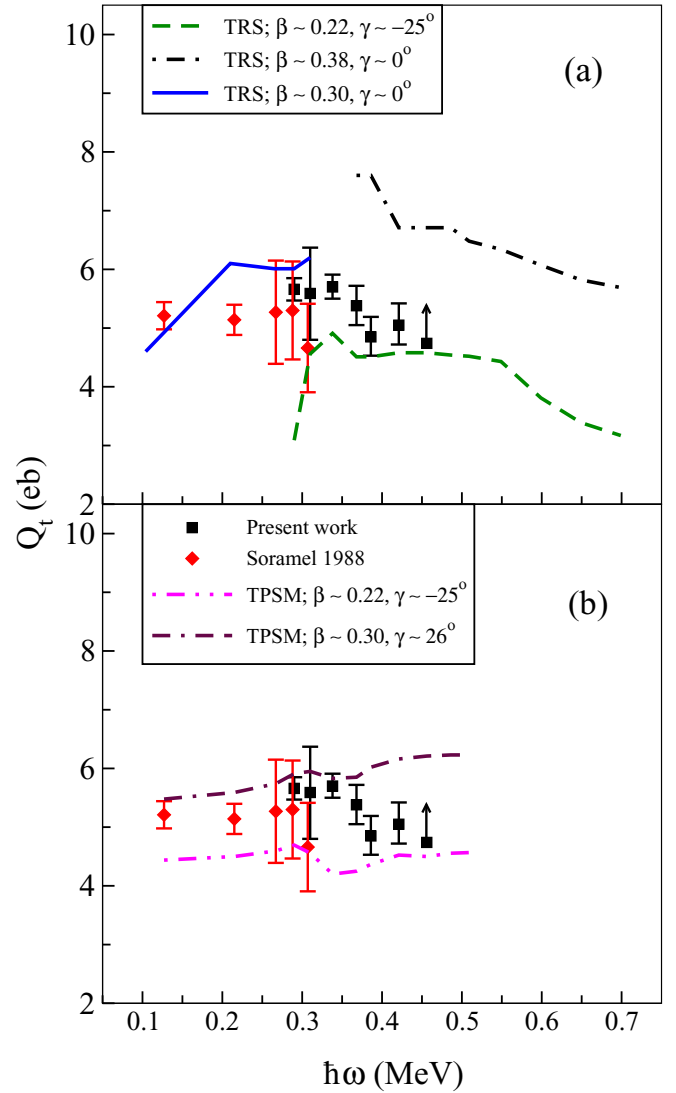


FIG. 8. The comparison of the theoretically (TRS and TPSM) calculated Q_t values with the measured values for the quadrupole band QB I in ^{136}Sm . The solid, dashed, and dot-dashed lines with indicated β and γ values correspond to (a) TRS calculations in top panel and (b) the dot-dot-dashed and dash-dash-dotted lines with indicated β and γ values correspond to TPSM values in bottom panel. Experimental Q_t values for low spin states (up to $I^\pi = 10^+$), shown by the filled diamonds, were taken from earlier work of F. Soramel *et al.* [14]. Measured Q_t values from present work are shown by filled squares.

the calculations could not reproduce a few values just beyond the first crossing ($I^\pi = 12^+$ and 14^+). Because the measured values are limited up to $I^\pi = 20^+$, we cannot extend the comparison to more higher-spin states after the second crossing ($\omega \approx 0.500$ MeV), where the calculated values exhibit three shapes, viz., oblate, triaxial, and highly deformed prolate. Additional lifetime measurements are required to probe the coexistence of multiple shapes after the second band crossing. The results clearly indicate, however, that the γ -soft shape ($\beta_2 \approx 0.30$ and $\gamma \approx 0^\circ$) at lower spins changes to the triaxial deformed shape ($\beta_2 \approx 0.22$ and $\gamma \approx -25^\circ$) with

the axis of rotation about the intermediate axis after spin $I^\pi \approx 10^+$.

It may be noted that the Q_i values of the lower-lying levels of ground state band in ^{134}Nd , an isotone of ^{136}Sm , were also reported as decreasing with spin and in agreement with the predictions of both the rotor model and the $O(6)$ symmetry of the interacting boson approximation. However, owing to the inconsistencies for higher states, strong change in deformations was suggested [27]. On the other hand, large reduction in collectivity was predicted by the projected shell model calculations [28].

B. Triaxial projected shell model approach

It is now well recognized that the TPSM approach provides a good description of the high-spin properties of well-deformed and transitional nuclei. The advantage of the TPSM approach is that the properties of heavy nuclei can be calculated with minimal computational effort. Further it allows for investigation not only of the ground-state band but also of the excited band structures around the optimum mean field. In the TPSM approach, the optimal mean field is the triaxial Nilsson potential, with the deformation parameters chosen either from the experimental data, if available, or from other theoretical approaches. To incorporate the pairing correlations, BCS calculations are performed with Nilsson single-particle energies. These Nilsson + BCS states are then projected onto good angular momentum states using an explicit three-dimensional angular-momentum projection operator.

In TPSM calculations, we employ the pairing plus quadrupole-quadrupole Hamiltonian [29]:

$$\hat{H} = \hat{H}_0 - \frac{1}{2}\chi \sum_{\mu} \hat{Q}_{\mu}^{\dagger} \hat{Q}_{\mu} - G_M \hat{P}^{\dagger} \hat{P} - G_Q \sum_{\mu} \hat{P}_{\mu}^{\dagger} \hat{P}_{\mu}, \quad (4)$$

with the last term in Eq. (4) being the quadrupole-pairing force. In Eq. (4), \hat{H}_0 is the spherical single-particle Hamiltonian, which contains a proper spin-orbit force [29]. The interaction strengths are taken as follows: The QQ -force strength χ is adjusted such that the physical quadrupole deformation ϵ is obtained as a result of the self-consistent mean-field Hartree-Fock-Bogolyubov calculation [29]. The monopole pairing strength G_M is of the standard form

$$G_M = \left(G_1 \mp G_2 \frac{N-Z}{A} \right) \frac{1}{A} \text{ (MeV)}, \quad (5)$$

where $-(+)$ is for neutron (proton). In the present calculation, we consider $G_1 = 20.12$ and $G_2 = 13.13$, which approximately reproduce the observed odd-even mass difference and this choice of G_M is appropriate for the single-particle space employed in the model, where three major shells are used for each type of nucleon ($N = 3, 4$, and 5 for both neutrons and protons). The quadrupole pairing strength G_Q is assumed to be proportional to G_M , and the proportionality constant is set equal to 0.16 [30–33].

The wave function is then used to evaluate the electromagnetic transition probabilities. The reduced electric transition probabilities $B(EL)$ from an initial state (σ_i, I_i) to a final state

(σ_f, I_f) are given by

$$B(EL, I_i \rightarrow I_f) = \frac{1}{2I_i + 1} |\langle \Psi_{I_f}^{\sigma_f} | \hat{Q}_L | \Psi_{I_i}^{\sigma_i} \rangle|^2, \quad (6)$$

and the reduced matrix element can be expressed as

$$\begin{aligned} & \langle \Psi_{I_f}^{\sigma_f} | \hat{Q}_L | \Psi_{I_i}^{\sigma_i} \rangle \\ &= \sum_{K_i, K_f} f_{I_i, K_i}^{\sigma_i} f_{I_f, K_f}^{\sigma_f} \sum_{M_i, M_f, M} (-)^{I_f - M_f} \begin{pmatrix} I_f & L & I_i \\ -M_f & M & M_i \end{pmatrix} \\ & \times \langle \Phi | \hat{P}_{K_f, M_f}^{I_f} \hat{Q}_{LM} \hat{P}_{K_i, M_i}^{I_i} | \Phi \rangle \\ &= 2 \sum_{K_i, K_f} f_{I_i, K_i}^{\sigma_i} f_{I_f, K_f}^{\sigma_f} \\ & \times \sum_{M', M''} (-)^{I_f - K_f} (2I_f + 1)^{-1} \begin{pmatrix} I_f & L & I_i \\ -K_f & M' & M'' \end{pmatrix} \\ & \times \int d\Omega D_{M'' K_i}(\Omega) \langle \Phi | \hat{Q}_{LM} \hat{R}(\Omega) | \Phi \rangle. \end{aligned}$$

The transition quadrupole moment $Q_i(I)$ is related to the $B(E2)$ transition probability through

$$Q_i(I) = \sqrt{\frac{16\pi}{5}} \frac{\sqrt{B(E2, I \rightarrow I-2)}}{\langle I, 0, 2, 0 | I-2, 0 \rangle}. \quad (7)$$

In the calculation, we have used the standard effective charges of $1.5e$ for protons and $0.5e$ for neutrons [34].

The TPSM calculations were performed with $\beta_2 = 0.3$ and $\gamma = 26^\circ$ and the corresponding band diagram is displayed in Fig. 9(a). The axial deformation has been adopted from the TRS calculations presented in the previous section. Although TRS results predict the axial shape at low-spin, nonaxial deformation has been used in TPSM study to reproduce the observed γ band. For low triaxial deformation values, the γ bandhead with $I^\pi = 2^+$, is located at high-excitation energy. For example, with $\gamma = 3^\circ$, the γ bandhead is located at 0.956 MeV with respect to the ground state. The γ bandhead is lowered in energy with increasing γ deformation keeping the value of β_2 constant at 0.3 . In particular, with $\gamma = 26^\circ$ the experimental γ bandhead is nearly reproduced. Similar lowering of the γ bandhead with increasing triaxiality has also been reported in our earlier work [30,31], and for the axial shape, the γ band is not possible in the projected shell model approach. It is evident from the band diagram that the first band crossing occurs at $I^\pi = 12^+$, which is due to the alignment of two quasiprotons. This corresponds to the first alignment observed in the experimental data and is also in agreement with the cranking calculations presented in the previous section. The second alignment observed in the experimental data is not reproduced in the band diagram. However, it is noted from the TRS results that a shape transition occurs after the first crossing and since the mean field is held fixed in the TPSM calculations, the results above the first crossing are inappropriate for this case.

For a correct description of the high-spin states above the band crossing, TPSM calculations have also been performed with the TRS minimum of $\beta = 0.22$ and $\gamma = 25^\circ$ and the projected bands are plotted in Fig. 9(b). It is evident from

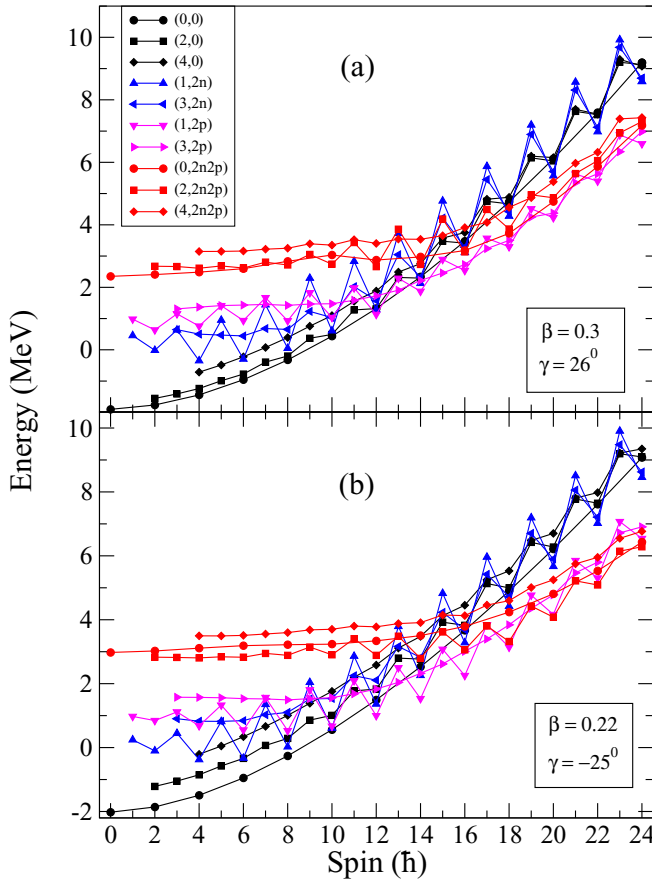


FIG. 9. Level energies are plotted against the spin for various configurations for sets of deformation parameters (a) $\beta = 0.3$ and $\gamma = 26^\circ$ and (b) $\beta = 0.22$ and $\gamma = -25^\circ$. The legend $(K, n\text{-qp})$ corresponds to the projected band from the n -qp state with K quantum number. For instance, $(2,0)$ corresponds to the projected band with $K = 2$ from the vacuum configuration and $(0, 2n2p)$ corresponds to the projected band with $K = 0$ from the two-neutron plus two-proton configuration.

the band diagram that a four-quasiparticle band (two protons and two neutrons) crosses the two-quasiparticle proton band at $I = 20$ and reproduces the second crossing observed in the experimental data.

Projected bands depicted in Fig. 9 and many more bands around the Fermi surface are then used to diagonalize the shell model Hamiltonian consisting of pairing plus the quadrupole-quadrupole interaction of Eq. (4). In the present study of ^{136}Sm , the number of projected states used in the calculations was 40. The calculated energies, with the subtracted core contribution, for the yrast and the γ bands are depicted in Figs. 10(a) and 10(b) for the two deformation parameter values discussed above. It is evident from the figure that below the band-crossing region, the mean field with deformations of $\beta = 0.3$ and $\gamma = 26^\circ$ gives a better description; however, above the crossing the mean field with $\beta_2 = 0.22$ and $\gamma = -25^\circ$ displays a better agreement with the experimental data. These calculations, therefore, substantiate the TRS prediction that this nucleus undergoes a shape transition at the band crossing. Additionally, the γ band does not show any

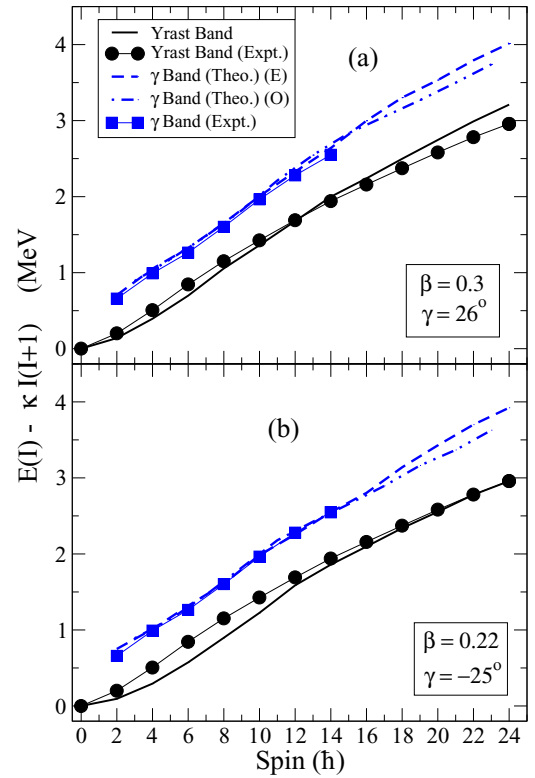


FIG. 10. Comparison of experimentally observed level energies of yrast and γ -vibration rotational bands with the values obtained from TPSM calculations. The experimental level energies of the yrast band agree well with the calculations (a) for $I^\pi < 16^+$ with $\beta = 0.3$ and $\gamma = 26^\circ$ and (b) for $I^\pi > 12^+$ with $\beta = 0.22$ and $\gamma = -25^\circ$. The γ band is insensitive to β values, suggesting that it only depends on triaxial γ deformation. Due to staggering in the γ band for high-spin states, TPSM energies of this band are shown separately for even-spin states (denoted by “E”) and odd-spin states (denoted by “O”).

significant change with respect to β_2 deformation as evident from Figs. 10(a) and 10(b).

Further, transition quadrupole moments, Q_t have been evaluated using the TPSM wave functions with effective charges of ($e_\pi = 1.5e$ and $e_v = 0.5e$). The TPSM results are shown in Fig. 8(b) along with the experimental data. It is noted from the figure that the measured Q_t values for low-spin states up to $I^\pi = 12^+$ are well reproduced with TPSM results with deformation parameters $\beta_2 = 0.3$ and $\gamma = 26^\circ$. There is a sudden drop in the experimental Q_t values beyond $I^\pi = 12^+$ that could not be explained with the chosen deformation of $\beta_2 = 0.3$ and $\gamma = 26^\circ$. The TPSM results with $\beta_2 = 0.22$ and $\gamma = -25^\circ$, which reproduce the band crossing behavior, qualitatively explain the drop in the measured Q_t values for higher-spin states beyond $I^\pi = 12^+$. However, the calculated values slightly underestimate the experimental Q_t values for states with $I^\pi = 14^+$, 16^+ , and 20^+ states. These comparisons further suggest that the system undergoes a shape transition along the yrast line around $I^\pi = 12^+$ due to particle alignment.

Thus, the measured Q_t values of the ground-state band along with both the theoretical calculations (TRS and TPSM)

presented here confirm that the yrast band, built on a γ -soft minimum at low spin, evolves into a triaxial deformed shape after the first band crossing. The reduction of collectivity with increasing spin after the band crossing is associated with the reduction of β_2 in the mean field of both the calculations. The γ -soft shape of ^{136}Sm at lower spin changes to the triaxial deformed shape ($\beta_2 \approx 0.22$ and $\gamma \approx -25^\circ$), with the axis of rotation about the intermediate axis, after spin $I^\pi = 10^+$. The γ -softness of the low-frequency minimum is consistent with the low-excitation energy of the γ -vibrational band built on the 2^+ state. It is important to note that the minimum at low- ω value is more γ -soft compared to the minimum after the particle alignment. This study confirms the evolution of shape from γ -soft to stable triaxial deformation in ^{136}Sm . Such shape evolution for even-even nuclei from γ -soft to stable triaxiality is important from the point of view of investigating chiral rotation at high spin and remains a subject of current interest in the field [35].

IV. CONCLUSIONS

Lifetimes of seven levels (up to $I^\pi = 20^+$) in the positive-parity yrast band have been measured in ^{136}Sm . A sudden drop has been observed in the measured Q_t values beyond $I^\pi = 12^+$. This reduction of collectivity has been reproduced by both theoretical calculations (TRS and TPSM) presented here and is seen as a consequence of a change in the nuclear shape.

Comparison of experimental transitional quadrupole moment (Q_t) values with the results of TRS and TPSM calculations suggests that ^{136}Sm evolves from a γ -soft shape before the first band crossing to a rigid triaxial shape ($\beta_2 \approx 0.22$, $\gamma \approx -25^\circ$). The occurrence of the first band crossing ($I^\pi = 12^+$) has been attributed to the alignment of two quasiprotons, while the second crossing arises from the alignment of both quasiproton and quasineutron pairs. The consistency of both theoretical models and their agreement with the measured values confirms a stable triaxial shape for ^{136}Sm after the band crossing. A strong case is made for further investigation of high-spin states in ^{136}Sm to search for chiral rotation at high spin.

ACKNOWLEDGMENTS

The help and cooperation of the INGA Collaboration in setting up the array is acknowledged. Technical help provided by S. Jadhav, B. S. Naidu, R. D. Donthi, and Abraham T. Vazhappilly during the preparation of the experiment is acknowledged. The authors are grateful to the staff at TIFR-BARC Pelletron Linac Facility for providing a consistent good quality beam and smooth operation of the accelerator for the entire duration of the experiment. The authors thank Dr. G. Mukherjee for useful discussion. This work has been partially funded by the Department of Science and Technology, Government of India (Grant No. IR/S2/PF-03/2003-II), and the U.S. National Science Foundation (Grant No. PHY-1713857).

-
- [1] P. Möller, R. Bengtsson, B. G. Carlsson, P. Olivius, and T. Ichikawa, *Phys. Rev. Lett.* **97**, 162502 (2006).
 - [2] S. Frauendorf, *Rev. Mod. Phys.* **73**, 463 (2001).
 - [3] F. L. Bello Garrote *et al.*, *Phys. Rev. C* **92**, 024317 (2015).
 - [4] M. A. Cardona, S. Lunardi, D. Bazzacco, G. de Angelis, and V. Roca, *Phys. Rev. C* **44**, 891 (1991).
 - [5] J. Xiang, Z. P. Li, W. H. Long, T. Nikšić, and D. Vretenar, *Phys. Rev. C* **98**, 054308 (2018).
 - [6] E. S. Paul, S. Davis, P. Vaska, P. J. Bishop, S. A. Forbes, D. B. Fossan, Y.-J. He, J. R. Hughes, I. Jenkins, Y. Liang, R. Ma, M. S. Metcalfe, S. M. Mullins, P. J. Nolan, R. J. Poynter, P. H. Regan, R. Wadsworth, and N. Xu, *J. Phys. G: Nucl. Part. Phys.* **19**, 861 (1993).
 - [7] C. J. Lister, B. J. Varley, R. Moscrop, W. Gelletly, P. J. Nolan, D. J. G. Love, P. J. Bishop, A. Kirwan, D. J. Thornley, L. Ying, R. Wadsworth, J. M. O'Donnell, H. G. Price, and A. H. Nelson, *Phys. Rev. Lett.* **55**, 810 (1985).
 - [8] M. Klintefjord *et al.*, *Phys. Rev. C* **93**, 054303 (2016).
 - [9] T. Nikšić, P. Ring, D. Vretenar, Y. Tian, and Z.-yu Ma, *Phys. Rev. C* **81**, 054318 (2010).
 - [10] A. Charvet *et al.*, *Z. Phys. A* **321**, 697 (1985).
 - [11] B. D. Kern, R. L. Mlekodaj, G. A. Leander, M. O. Kortelahti, E. F. Zganjar, R. A. Braga, R. W. Fink, C. P. Perez, W. Nazarewicz, and P. B. Semmes, *Phys. Rev. C* **36**, 1514 (1987).
 - [12] E. S. Paul, C. W. Beausang, R. M. Clark, S. A. Forbes, A. Gizon, J. Gizon, K. Hauschild, I. M. Hibbert, P. J. Nolan, D. Santos, A. T. Semple, J. Simpson, R. Wadsworth, L. Walker, and J. N. Wilson, *J. Phys. G: Nucl. Part. Phys.* **20**, 1405 (1994).
 - [13] N. J. O'Brien, R. Wadsworth, D. E. Archer, P. Fallon, I. M. Hibbert, D. T. Joss, D. R. LaFosse, P. J. Nolan, E. S. Paul, J. Pfohl, M. A. Riley, D. G. Sarantites, and R. Wyss, *Phys. Rev. C* **58**, 3212 (1998).
 - [14] F. Soramel, S. Lunardi, S. Beghini, M. Morando, C. Signorini, W. Meczynski, G. Fortuna, G. Montagnoli, and A. M. Stefanini, *Phys. Rev. C* **38**, 537 (1988).
 - [15] R. Wadsworth, J. M. O'Donnell, D. L. Watson, P. J. Nolan, P. J. Bishop, D. J. Thornley, A. Kirwan, and D. J. G. Love, *J. Phys. G: Nucl. Phys.* **13**, 205 (1987).
 - [16] A. Makishima, M. Adachi, H. Taketani, and M. Ishii, *Phys. Rev. C* **34**, 576 (1986).
 - [17] K. S. Vierinen, J. M. Nitschke, P. A. Wilmarth, R. B. Firestone, and J. Gilat, *Nucl. Phys. A* **499**, 1 (1989).
 - [18] H. Tan *et al.*, in *Proceedings of the IEEE Nuclear Science Symposium and Medical Imaging Conference (2008NSS/MIC)*, Dresden (IEEE, New York, 2009), p. 2471.
 - [19] R. Palit, S. Saha, J. Sethi, T. Trivedi, S. Sharma, B. S. Naidu, S. Jadhav, R. Donthi, P. B. Chavan, H. Tan *et al.*, *Nucl. Instrum. Methods Phys. Res., Sect. A* **680**, 90 (2012).
 - [20] D. C. Radford, *Nucl. Instrum. Methods Phys. Res., Sect. A* **361**, 297 (1995).
 - [21] N. R. Johnson, J. C. Wells, Y. Akovali, C. Baktash, R. Bengtsson, M. J. Brinkman, D. M. Cullen, C. J. Gross, H.-Q. Jin, I.-Y. Lee, A. O. Macchiavelli, F. K. McGowan, W. T. Milner, and C.-H. Yu, *Phys. Rev. C* **55**, 652 (1997).
 - [22] L. C. Northcliffe and R. F. Schilling, *At. Data Nucl. Data Tables* **7**, 233 (1970).

- [23] S. Rajbanshi, A. Bisoi, S. Nag, S. Saha, J. Sethi, T. Trivedi, T. Bhattacharjee, S. Bhattacharyya, S. Chattopadhyay, G. Gangopadhyay, G. Mukherjee, R. Palit, R. Raut, M. Saha Sarkar, A. K. Singh, and A. Goswami, *Phys. Rev. C* **89**, 014315 (2014).
- [24] S. Rajbanshi, A. Bisoi, S. Nag, S. Saha, J. Sethi, T. Bhattacharjee, S. Bhattacharyya, S. Chattopadhyay, G. Gangopadhyay, G. Mukherjee, R. Palit, R. Raut, M. Saha Sarkar, A. K. Singh, T. Trivedi, and A. Goswami, *Phys. Rev. C* **90**, 024318 (2014).
- [25] W. Nazarewicz, J. Dudek, R. Bengtsson, T. Bengtsson, and I. Ragnarsson, *Nucl. Phys. A* **435**, 397 (1985).
- [26] W. Nazarewicz, M. A. Riley, and J. D. Garrett, *Nucl. Phys. A* **512**, 61 (1990).
- [27] T. Klemme, A. Fitzler, A. Dewald, S. Schell, S. Kasemann, R. Kühn, O. Stuch, H. Tiesler, K. O. Zell, P. von Brentano, D. Bazzacco, F. Brandolini, S. Lunardi, C. M. Petrache, C. Rossi Alvarez, G. De Angelis, P. Petkov, and R. Wyss, *Phys. Rev. C* **60**, 034301 (1999).
- [28] L.-J. Wang, Y. Sun, T. Mizusaki, M. Oi, and S. K. Ghorui, *Phys. Rev. C* **93**, 034322 (2016).
- [29] K. Hara and Y. Sun, *Int. J. Mod. Phys. E* **04**, 637 (1995).
- [30] J. A. Sheikh, G. H. Bhat, W. A. Dar, S. Jehangir, and P. A. Ganai, *Phys. Scr.* **91**, 063015 (2016).
- [31] S. Jehangir, G. H. Bhat, J. A. Sheikh, R. Palit, and P. A. Ganai, *Nucl. Phys. A* **968**, 48 (2017).
- [32] J. A. Sheikh and K. Hara, *Phys. Rev. Lett.* **82**, 3968 (1999).
- [33] Y. Sun, K. Hara, J. A. Sheikh, J. G. Hirsch, V. Velazquez, and M. Guidry, *Phys. Rev. C* **61**, 064323 (2000).
- [34] J. A. Sheikh, G. H. Bhat, Y.-X. Liu, F.-Q. Chen, and Y. Sun, *Phys. Rev. C* **84**, 054314 (2011).
- [35] B. F. Lv *et al.*, *Phys. Rev. C* **98**, 044304 (2018).